

**Influence on open-circuit voltage by optical heterogeneity in three-dimensional organic photovoltaics**Yuan Li,<sup>1</sup> Mingjun Wang,<sup>1,3</sup> Huihui Huang,<sup>1,3</sup> Wanyi Nie,<sup>1</sup> Qi Li,<sup>2</sup> Eric D. Peterson,<sup>1</sup> Robert Coffin,<sup>1</sup> Guojia Fang,<sup>3</sup> and David L. Carroll<sup>1,\*</sup><sup>1</sup>*Center for Nanotechnology and Molecular Materials, Department of Physics, Wake Forest University, Winston-Salem, NC 27109, USA*<sup>2</sup>*Department of Physics, Wake Forest University, Winston-Salem, NC 27109, USA*<sup>3</sup>*Key Laboratory of Artificial Micro- and Nano-structures of Ministry of Education, Department of Electronic Science and Technology, School of Physics and Technology, Wuhan University, Wuhan, Hubei 430072, P. R. China*

(Received 19 April 2011; revised manuscript received 28 June 2011; published 24 August 2011)

In three-dimensional photovoltaic architectures, heterogeneous optical intensity distributions throughout the structure may generally lead to modifications to the short circuit current density ( $J_{sc}$ ), open-circuit voltage ( $V_{oc}$ ), and fill factor (FF). In this work an equivalent circuit model has been developed to examine the impact on  $V_{oc}$  by heterogeneous and homogeneous internal illumination. The model has been tested against data from planar cell and tube-based solar cells that utilize poly-(3-hexylthiophene): phenyl C61 butyric acid methyl ester (P3HT:PCBM). This has further been extended to predict optimum optical design for tube-based geometries in which organic photoconversion materials have been applied in both fabrication conditions. The result is that for such geometries to provide the best overall optical confinement and best power conversion performance, aspect ratios must be between 1 and 5. The resulting structure leads to best light capture together with best overall internal partitioning of optical power to achieve the highest possible  $V_{oc}$ .

DOI: [10.1103/PhysRevB.84.085206](https://doi.org/10.1103/PhysRevB.84.085206)

PACS number(s): 72.40.+w

**I. INTRODUCTION**

Organic photovoltaics (OPVs) traditionally do not perform as well as their inorganic counterparts for two important reasons: (1) they lack sufficient spectral overlap with the sun and (2) they have low carrier mobility. While the photovoltaics community has seen tremendous progress in the spectral overlap problem recently with the advent of low band gap polymers,<sup>1–5</sup> the problem of charge carrier mobility has been difficult to overcome. The mobility issue typically necessitates the use of thin-film absorbers (70 nm–150 nm), and this can reduce the total light that is absorbed.<sup>6,7</sup> To address these issues, several types of three-dimensional (3D) architectures have been proposed that provide confinement of the optical field resulting in extremely long optical paths within the device for optimized absorption. Optical confinement geometry organic photovoltaics (OCGOPV) such as fiber-based PV,<sup>8–10</sup> tube-based PV,<sup>11</sup> fiber bundle PV,<sup>12</sup> stamped fiber PV,<sup>12</sup> fiber nanowire hybrid dye-sensitized PV,<sup>13</sup> and others,<sup>14–18</sup> have been intensely studied recently. Some examples are shown in Fig. 1.

A particularly attractive feature of such geometries is that it is possible to fabricate an efficient cell using ultrathin organic thin films (lower than 50 nm) and thereby lead to high filling factors due to decreased recombination.<sup>19–21</sup> Further, due to the well-defined mode structure of many of these geometries, there is the possibility of effectively utilizing frequency conversion schemes. Because of the long optical path in fiber, a frequency converter can play an effective role in doubling high-energy photo to improve current. However, there are still several problems that must be overcome. Recently, we reported that the open-circuit voltage ( $V_{oc}$ ) tends to decrease in OCGOPV geometries.<sup>11,12</sup> In that earlier work, we defined two “active” areas of the general 3D geometry as in Fig. 2(a): the “Current Active Area” (CAA), which is the area from which current is collected and the “Illumination Active Area” (IAA), which is the area of illumination of the structure.<sup>11</sup>

These are a distinctive feature of any OCGOPV. Essentially for the planar cell, IAA equals CAA, but in the OCGOPV, the CAA is much greater than the IAA. In other words the flux entering the aperture (IAA) is spread over a much larger area within the cell (the CAA) leading to a lower optical intensity on CAA like an inverse concentrator. Because light is generally partitioned into modes of the “confining cavity,” the optical intensity in an OCGOPV is typically heterogeneously distributed across the CAA (HeOI), differing from the homogeneous optical intensity (HoOI) in planar OPV. The heterogeneous distribution in OCGOPVs can be simulated by ray tracing model we reported<sup>9</sup> as shown in Fig. 2(b). If this power heterogeneity becomes too great, a loss in  $V_{oc}$  will occur for the device. In this paper, we examine the effects of optical heterogeneity on a model OCGOPV using a composite equivalent circuit analysis.

**II. THEORY**

To understand the performance of an OCGOPV, it is necessary to know the connections between their electrical and optical characteristics. First, as shown in Fig. 3(a), we take a small piece from a whole OCGOPV (a.1) as one *subunit* (a.2) and treat it like a planar solar cell (a.3). For each *subunit* in (a.2), when very small, we may assume it fits planar cell theory. In Fig. 3(b), the equivalent circuit of planar cell is described by J-V characteristics expressed by the generalized Shockley equation<sup>22–24</sup>

$$J = \frac{R_p}{R_s + R_p} \left\{ J_s \left[ \exp \left( \frac{e(V - J R_s)}{n_D k_B T} \right) - 1 \right] + \frac{V}{R_p} \right\} - J_{ph} + J_{Rec} \quad (1)$$

where,  $n_D$  is the diode ideality factor,  $J_s$  is the reverse saturation current, and  $J_{Rec}$  is represented by the current source, which counteracts the photocurrent  $J_{ph}$ .<sup>25–27</sup> Due to

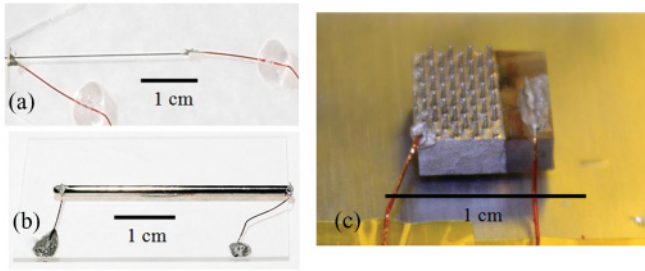


FIG. 1. (Color online) (a) Fiber-based solar cell. (b) Tube-based solar cell. (c) Aligned plastic fiber cell with different diameter and length

lower carrier mobility in polymers generally,<sup>28–30</sup> the main factors influencing the recombination rate  $r_{\text{Rec}}$ , are thickness of polymer, the temperature, and the fabrication procedure and polymer processing used. For very thin films of bulk heterojunction polymer blends, the influence of  $r_{\text{Rec}}$  on  $J_{\text{sc}}$  can be safely ignored.<sup>19</sup>

To account for heterogeneity in the OCGOPVs, the model must consist of many OPV *subunits* with different performances, as shown in Fig. 3(c). They absorb different photon numbers to contribute many  $j_i$ , and each generates a different  $v_i$ . The contributions from the individual cells are summed to provide a whole  $J_{\text{ph}}$  and  $V_D$  as show below.

$$J_{\text{ph}} = \frac{1}{n} \sum_{i=1}^n j_i = \frac{1}{n} \sum_{i=1}^n \int \frac{e\lambda}{hc} \eta(\lambda) Q_i(\lambda) d\lambda \quad (2)$$

Where,  $Q_i(\lambda)$  is the spectral irradiance on the active area from the incident light at each *subunit*, which can be obtained by a 3D fiber-cell model based on ray tracing<sup>9</sup> coupled with a transfer matrix method, which accounts for the materials absorption properties.<sup>19,20,31,32</sup> In Eq. (2),  $h$ ,  $c$ ,  $e$ , and  $\lambda$  are the Planck’s constant, light speed, electron charge, and wavelength.  $\eta(\lambda)$  is the external quantum efficiency of wavelength  $\lambda$ . From Eq. (1),

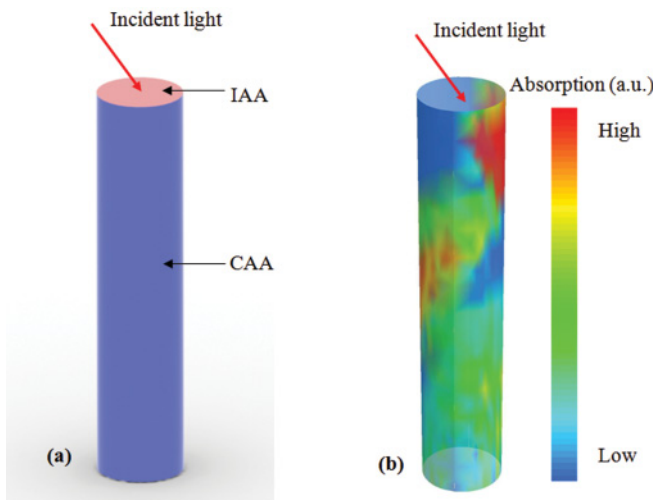


FIG. 2. (Color online) (a) IAA and CAA are represented as pink area (light gray) at the top and blue area (dark gray) surround the fiber. (b) Heterogeneous absorption distribution through inner surface in OCGOPVs is simulated by a ray tracing model.<sup>9</sup> The legend at the right represents the absorption level at inner surface.

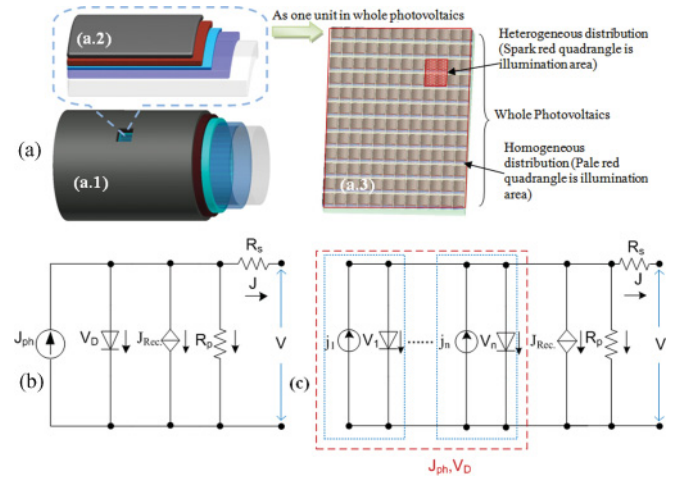


FIG. 3. (Color online) (a) From (a.1) to (a.3), our model divides the OCGOPV into *subunits*, and then connects them as a planar photovoltaics. In (a.3), illumination across the *subcells* is heterogeneously distributed due to the mode structure of the waveguide. (b) The equivalent circuit of conventional planar OPV.  $J_{\text{ph}}$ ,  $r_{\text{Rec}}$ ,  $V_D$ ,  $R_s$ , and  $R_p$  are photocurrent source, recombination, diode voltage, series resistances, and parallel resistances, respectively.  $J$  and  $V$  are the output current density and voltage of OPV. (c) The equivalent circuit of the OCGOPVs composed of unit *subcells*.

when  $J = 0$ , the open-circuit voltage  $V_{\text{oc}} = V = V_D$ . Also since  $J_s R_p > V_{\text{oc}}$ ,<sup>26</sup> Eq. (2) can be simplified as

$$V_{\text{oc}} = \frac{n_D k_B T}{e} \ln \left( \frac{(R_p + R_s) J_{\text{ph}}}{J_s R_p} + 1 \right), \quad J_{\text{ph}} = \frac{1}{n} \sum_n j_i. \quad (3)$$

Equation (3) represents the case of homogeneous illumination when all  $j_i$  are equal. When the optical intensity is heterogeneous, i.e., each *subunit* cell absorbs different light fluxes and contributes various voltages, their superimposed voltage  $V_{\text{oc}}$  is described as the average of all voltage of unit *subcells* in Eq. (4).<sup>33,34</sup>

$$V_{\text{oc}} = \frac{1}{n} \sum_n V_i \quad (4)$$

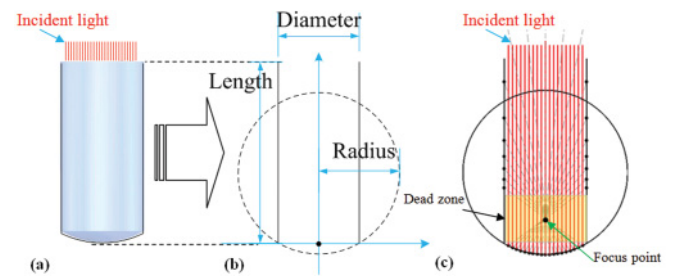


FIG. 4. (Color online) (a) The OCGOPV with a given curvature cap at the bottom. (b) Light path in longitudinal section of (a). A beam of light (red lines, distance to y axis is  $x$ ) enters into the tube (length  $h$ ) and reflects at points  $(x_1, y_1)$  on bottom of curvature radius  $r$ , then reaches the inner surface  $(x_2, y_2)$ . (c) There is a “dead zone” near bottom, where no light shines. Red lines (solid lines) are incident light paths, and gray lines (dashed lines) are reflected light paths.

$$V_i = \frac{n_D k_B T}{e} \ln \left( \frac{(R_p + R_s) j_i}{J_s R_p} + 1 \right). \quad (5)$$

When  $j_i$  is constant and equals the average current density of the whole cell, Eq. (5) becomes Eq. (3) of the homogeneous case. Using the calculus of variations, the  $V_{oc}$  dependence on the distribution  $j_i$  can be examined, and when  $j_s$  is much less than  $J_{ph}$ , the variation of  $\delta V_{oc}$  is written as below.<sup>34</sup>

$$\delta V_{oc} \approx \frac{0.026V}{x_0 j_{HoOI}} \int_0^{x_0} \delta j(x) dx \quad (6)$$

Where,  $x_0$  can be assumed to be a *subunit* area,  $j(x)$  can be regarded as the average current density  $j_{HoOI}$  in the homogeneous case, and  $\delta j(x)$  is the perturbation in the heterogeneous case. Since the total current is constant, i.e., the integral of the variation of current density  $\delta j(x)$  is 0,  $\delta V_{oc} = 0$ . For the cases of large variation of  $j(x)$ , the upper bound of  $V_{oc}$  of two cases are shown as Eq. (8).<sup>34</sup>

$$V_{oc-homo} - V_{oc-heter} \leq a \ln \left( \frac{2u(b + \mu)}{2u(b + \mu) - \sigma} \right) \quad (7)$$

$$a = \frac{n_D k_B T}{e}, \quad b = \frac{J_s R_p}{R_p + R_s}, \quad j(x) \in [u, v] \quad (8)$$

Where  $\mu$  is the average illumination power, and  $\sigma$  is the variance of illumination power. In most common distribution,  $2a(b + \mu) > \sigma$  for most device parameters,<sup>35</sup> therefore  $V_{oc-heter} - V_{oc-homo} \sim 0$ . Consequently, the total illumination, whether homogenous or heterogeneous illumination has the same functional effect on voltage. This will be examined in detail below.

Now, we expand this principle to the architecture of a real device. First, to know which variables are important and how they influence the optical power distributions, we consider a specific geometry such as one single waveguide such as a tube, which is shown in Fig. 4. As we have recently shown for fibers, and which also holds true for tubes,<sup>9</sup> the ratio of length to diameter can influence light absorption in the OCGOPVs, and as noted, this geometry also leads to a heterogeneous distribution of optical power in inner surface of this specific geometry. Further, there is a strong dependence of short-circuit current  $J_{sc}$ , on the incident angle at which the illumination is coupled. The optimum incident angle depends on this ratio of length to diameter of the structure.<sup>9,36</sup>

### III. EXPERIMENT

Tube-based solar cell is an extended fiber device with a hemisphere bottom. They were fabricated on glass tubes with one end closed in a hemispherical cap (Chemglass, 1 mm i.d.). The Indium Tin Oxides (ITO) films with a thickness of 100 nm were deposited on these *substrates* by radio frequency magnetron sputtering (BOSCH) from an ITO target (depositing 100 nm of ITO per 120° rotation, for three times). The *substrates* were then exposed to ozone for 90 min (rotating the tubes three times every after 30 min). Subsequently, by dip coating, the buffer layer and absorber layer were added. Poly(3,4-ethylenedioxythiophene)-poly(styrenesulfonate) (PEDOT:PSS, Clevios P, the film thickness is ~40 nm), and poly-(3-hexylthiophene:phenyl C<sub>61</sub> butyric acid methyl ester (P3HT:PCBM = 1:0.8 in weight

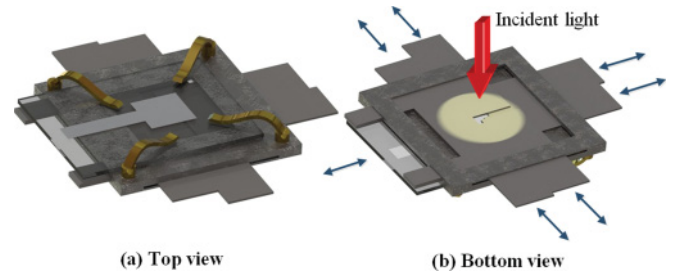


FIG. 5. (Color online) A tool for measuring heterogeneous distribution of solar light in a *subunit* of a planar device. Solar light comes from the bottom [red arrow (light arrows) in (b) shows the direction of solar light] and goes through the aperture hole for which the size could be adjusted by four panels [blue arrows (dark arrows) represent the adjustable directions of slices in (a)].

(WT) in chlorobenzene, of 15 mg/ml P3HT for planar cell, and 5 mg for tube devices) were deposited on the tube substrate. Finally, Al electrodes were deposited via thermal evaporation at the pressure of  $10^{-6}$  Torr. Similarly planar devices were fabricated using spin coating, for comparison purpose. Both devices were lightly annealed ( $\sim 100^\circ\text{C}$  for five min).

For both device types, the illumination intensity was varied to determine the performance as a function of illumination power. The case of heterogeneous illumination was simulated for the planar device by changing the area of illumination by a special mask, for a given luminous power. The architecture of this tool is shown in Fig. 5. The active area is  $0.5\text{ cm}^2$ . Current voltage characteristics were collected using Keithley 236 Source-Measurement Unit and an AM1.5g Standard Newport No. 96000 Solar Simulator. The output power intensity is adjusted from  $0.5\text{ mW/cm}^2$  to  $150\text{ mW/cm}^2$ .

To test the above model, three different types of organic photovoltaic cells were built. All are based on the P3HT:PCBM bulk heterojunction as described. Architectures and corresponding fabrication methods are shown in Table I.

### IV. RESULTS AND DISCUSSION

As shown above, both homogeneous and heterogeneous cases have the same functional dependence with voltage. If this is true, it will provide a simple method to study the global distribution of optical power in the OCGOPVs. First, we use an “ideal” planar device (sample A) to test the two illumination cases, shown in Fig. 6. As expected, both HeOI and HoOI show the same overall impact on the observed  $V_{oc}$ , as average input (at the front of the device) light intensity is lowered. Specifically, the  $V_{oc}$  drops sharply when input optical intensity is lower than  $\sim 10\text{ mW/cm}^2$ , which is also described by Eq. (3) above. In other words the variation of the voltage is the same for case in which only a small *subunit* is illuminated or the whole cell is illuminated. The gray curve is fitted by Eq. (3) in which all the parameters of devices are extracted from IV curve in terms of an iterative method.<sup>35</sup>

Then, we apply this principle into the tube-based cell (sample B), which were prepared by a dip-coating method. In this case, the normally incident light at the front face of the OCGOPV (sample B) is homogeneous, but it will be distributed throughout the volume heterogeneously, on the inner surface as in Fig. 1(d). In Fig. 6(b), we plot a planar OPV

TABLE I. Sample fabrication details.

Sample	Architecture	Fabrication method
A	Substrate/ITO/PEDOT/P3HT:PCBM/Al	Spin coating
B	Tube/ITO/PEDOT/P3HT:PCBM/Al	Dip coating
C	Substrate/ITO/PEDOT/P3HT:PCBM/Al	Dip coating

(sample C, fabricated using the same dip-coating procedure) together with the tube-based device. Because OCGOPVs have a very large CAA, i.e., the average optical intensity on the inner surface (CAA) is very low, the  $V_{oc}$  of the tube OPV tends to a lower voltage than planar devices as shown in green. To determine the average optical power inside the tube, the total incident flux was divided by the total internal area of the device. This effective heterogeneous intensity (red square, B) was used to *normalize* the  $V_{oc}$  to intensity. This normalized  $V_{oc}$  shows the same functional behavior in the OCGOPV as homogeneous illumination does in the control device (blue sphere, C).

To fully understand how this may modify the overall performance of the OCGOPV (the efficiency), we have also measured the filling factor and current collection for the planar device and compared it to the OCGOPV as a function of illumination intensity. Figure 7(a) shows the FF for the spin-cast device (sample A, our “ideal” device), the OCGOPV (sample B), and the dip-coating planar device (sample C). For the planar device fabricated with spin coating, there exists a peak in FF near  $10 \text{ W/m}^2$ . As is typical with such OPVs, the FF varies with the quality of the thin films, but it can be rather high (near 0.7). Generally, the FF of OCGOPV is also limited by the film quality. Since dip coating was used to fabricate tube-based cell, resulting in uneven films, the FF for both the dip-coated tube structures and planar structures drop. In the case of the tube device, it is approximately reduced by 0.25. The normalized FF of OCGOPV also shows the same functional behavior as homogeneous illumination does in dip coating the planar device (pink line, C). In terms of Eq. (1), J-V is simulated to find the maximum obtainable output power  $P_m$  and corresponding  $J_m$  and  $V_m$ , then the FFs of different

$J_{ph}$  are obtained as a gray line in Fig. 7(a) to compare with the experiment.

On the other hand, Fig. 7(b) illustrates that the OCGOPV can transfer more light flux to current than the conventional OPV. This has been previously reported in several publications.<sup>10,16,36</sup> Moreover, this advantage is enhanced with increasing optical illumination intensity at the entrance aperture. This suggests that OCGOPVs will perform well with high-illumination intensity applications such as concentrators.<sup>37–39</sup>

We can now examine the overall result of these effects on efficiency. The efficiency as a function of incident optical illumination intensity is shown in Fig. 8(a). For the planar cell (sample A, blue spheres), the optimum optical intensity of the highest efficiency is near  $10 \text{ mA/cm}^2$ , which is far less than the AM1.5g standard solar light ( $100 \text{ mW/cm}^2$ ) allows for P3HT:PCBM. That indicates the highest performance requires reducing the optical intensity. However, the tube-based cell (sample B) exhibits a monotonically increasing efficiency with optical intensity at the input aperture. This is because at the lowest values of IAA, the optical intensity within the device volume is very low. When the efficiency of the OCGOPV is scaled with the average internal illumination intensity given by CAA (shown in the yellow rectangle), the curve’s shape is similar with that of the planar cell of both spin cast and dip coat at lower optical intensity but performs better than that of planar cell of same dip-coating procedure (upper angle, C). This also suggests the functional equivalence of HoOI and HeOI in OPVs generally.

Using this “optical intensity effect,” we can predict the optimum efficiency of OCGOPVs, as a function of the geometry: ratios of the length/diameter of OCGOPV together with the ratios of bottom curvature radius to diameter (radius/diameter). Since the two fabrication procedures: dip-coating film and spin coating yield different film morphologies, we must also

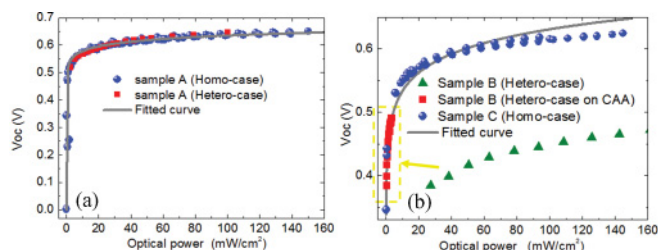


FIG. 6. (Color online) (a) The  $V_{oc}$  vs optical intensity of sample A, which is illuminated by simulated heterogeneous variation (red square) and homogeneous variation (blue sphere), respectively. The  $V_{oc}$  vs  $I$  curves are fitted to Eq. (3) and shown as the grey line. (b) The  $V_{oc}$  vs optical intensity for dip-coating devices. The curve with “on CAA” means the optical power of incident optical flux divided CAA.<sup>11</sup> Here, the red square and green triangle are the same illumination data divided by IAA and CAA, respectively.

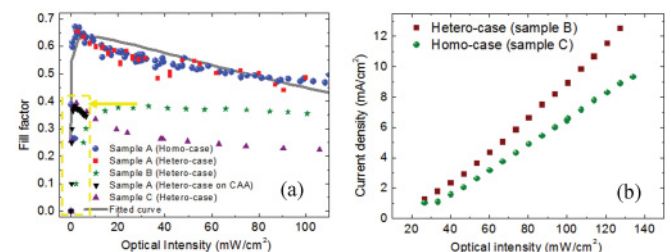


FIG. 7. (Color online) (a) FF vs optical intensity of sample A, sample B, and sample C. The green stars and the black down-triangles (in yellow rectangle) are the same input flux data divided by IAA and CAA, respectively. The gray line is the fitted curve by Eq. (1). (b)  $J_{sc}$  vs optical intensity (IAA) of planar and OCGOPV device with architecture ITO/PEDOT/P3HT:PCBM/Al.

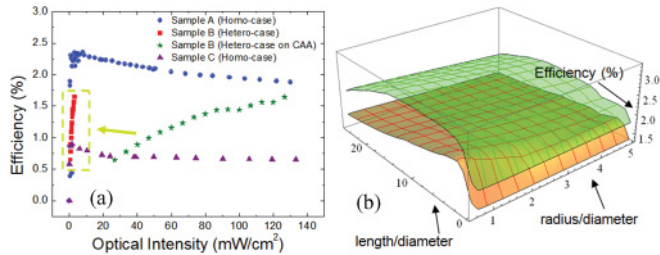


FIG. 8. (Color online) (a) Efficiency vs optical intensity of sample A, sample B, and sample C. The green stars and the red squares (in yellow rectangle) are the same input flux data divided by IAA and CAA, respectively. (b) The simulation of efficiency vs the ratio length/diameter of the tube and the ratio of bottom curvature radius and tube diameter is in the condition of normal incident light and for two fabrications of spin coating (green surface) and dip coating (orange surface). This simulation is based on an optical path method and a transfer matrix mentioned before<sup>9,31</sup> and also use the experiment data from the left Fig. 8(a).

consider this. In Fig. 8(b), we again use the tube-based cell as a typical case of OCGOPVs. The efficiency drops with the increase of the ratio of radius of bottom/diameter of tube, because of the reflection loss from the bottom reflector [see Fig. 4(c)], which we have termed “the dead zone” (when this ratio  $> 1/\sqrt{2}$ ). Moreover, the peak in the dimension of length/diameter is the combined result of current increase and voltage decrease. Longer OCGOPVs can absorb more light energy to generate a higher current density,<sup>9</sup> but it has a negative impact on voltage. This phenomenon is simulated for both film cases. The peaks are all with relatively low optical intensity ( $\ll 100$  mW/cm<sup>2</sup>) on the inner surface. Thus, the optimum design for OCGOPVs should be that the length/diameter is in the range of 1 to 5, and the curvature radius/diameter is between 0.5 and 0.7 for normal incidence, which the accurate ratio predictions depend on the film quality, thickness, and polymer type. Here for the tube-based geometries using P3HT:PCBM is located at length/diameter 2

and radius/diameter 0.7. This could explain why in the past research that the longer fiber devices were used to reach high photocurrent but leading to a lower voltage.<sup>11,18</sup>

## V. CONCLUSION

In this work we have examined the overall effect of 3D architectures on the performance of photovoltaic conversion. Specifically, we have provided an equivalent circuit equation of OCGOPVs by revising the Shockley equation to apply to the case of optical heterogeneity within the structure. Using this approach we have shown a functional equivalence of internal HoOI and HeOI for OPVs generally. The overall effect of optical heterogeneity on performance parameters in our model, 3D, fiber-based structure is that the Voc is lowered generally as the ratio of length to diameter becomes large. This corresponds to a large internal area of the device. Jsc is seen to increase substantially for large internal device areas, whereas the FF is less sensitive overall. We have correlated our model calculations to experimentally obtained values in a fiber device using P3HT:PCBM absorbers. Finally, it was found that there is an optimum design to the highest efficiency for tube-based OCGOPV, which corresponds to a length/diameter in the range of 1 to 5 and an optimum radius of bottom/diameter of tube lower than 0.7. These results suggest that realization of truly high performance devices utilizing polymers on 3D architectures will require new polymer systems capable of maintaining higher voltages under lower light conditions.

## ACKNOWLEDGMENTS

The authors gratefully acknowledge funding from AFOSR Grants No. FA9550-04-1-0161 and DOE No. DE-FG02-07ER46428. Finally, we would like to thank Xiao Xu for assistance in getting the photograph shown in Fig. 1 and thank Dan Xue for helping to develop the software OPVAP<sup>40</sup> simulation platform, and also thank Xiang Wan for his assistance in mathematics.

\*Corresponding author: carrolld@wfu.edu

- <sup>1</sup>X. Gong, M. Tong, Y. Xia, W. Cai, J. S. Moon, Y. Cao, G. Yu, C.-L. Shieh, B. Nilsson, and A. J. Heeger, *Science* **325**, 1665 (2009).
- <sup>2</sup>J. Y. Kim, K. Lee, N. E. Coates, D. Moses, T. Q. Nguyen, M. Dante, and A. J. Heeger, *Science* **317**, 222 (2007).
- <sup>3</sup>S. H. Park, A. Roy, S. Beaupre, S. Cho, N. Coates, J. S. Moon, D. Moses, M. Leclerc, K. Lee, and A. J. Heeger, *Nat. Photonics* **3**, 297 (2009).
- <sup>4</sup>R. C. Coffin, J. Peet, J. Rogers, and G. C. Bazan, *Nat. Chem* **1**, 657 (2009).
- <sup>5</sup>H. Y. Chen, J. H. Hou, S. Q. Zhang, Y. Y. Liang, G. W. Yang, Y. Yang, L. P. Yu, Y. Wu, and G. Li, *Nat. Photonics* **3**, 649 (2009).
- <sup>6</sup>C. J. Brabec, N. S. Sariciftci, and J. C. Hummelen, *Adv. Funct. Mater.* **11**, 15 (2001).
- <sup>7</sup>K. M. Coakley and M. D. McGehee, *Chem. Mater.* **16**, 4533 (2004).

- <sup>8</sup>J. W. Liu, M. A. G. Namboothiry, and D. L. Carroll, *Appl. Phys. Lett.* **90**, 063501 (2007).
- <sup>9</sup>Y. Li, W. Zhou, D. Xue, J. Liu, E. D. Peterson, W. Nie, and D. L. Carroll, *Appl. Phys. Lett.* **95**, 203503 (2009).
- <sup>10</sup>B. O'Connor, K. P. Pipe, and M. Shtein, *Appl. Phys. Lett.* **92**, 193306 (2008).
- <sup>11</sup>Y. Li, E. D. Peterson, H. Huang, M. Wang, D. Xue, W. Nie, W. Zhou, and D. L. Carroll, *Appl. Phys. Lett.* **96**, 243505 (2010).
- <sup>12</sup>Y. Li, W. Nie, J. Liu, A. Partridge, and D. L. Carroll, *IEEE J. Select. Topics Quantum Electron.* **16**, 1 (2010).
- <sup>13</sup>B. Weintraub, Y. G. Wei, and Z. L. Wang, *Angew. Chem. Int. Ed. Engl.* **48**, 8981 (2009).
- <sup>14</sup>X. Fan, F. Wang, Z. Chu, L. Chen, C. Zhang, and D. Zou, *Appl. Phys. Lett.* **90**, 073501 (2007).
- <sup>15</sup>S. Curran, J. Talla, S. Dias, and J. Dewald, *J. Appl. Phys.* **104**, 064305 (2008).

- <sup>16</sup>M. R. Lee, R. D. Eckert, K. Forberich, G. Dennler, C. J. Brabec, and R. A. Gaudiana, *Science* **324**, 232 (2009).
- <sup>17</sup>X. Fan, Z. Z. Chu, F. Z. Wang, C. Zhang, L. Chen, Y. W. Tang, and D. C. Zou, *Adv. Mater.* **20**, 592 (2008).
- <sup>18</sup>H. Huang, Y. Li, M. Wang, W. Nie, W. Zhou, E. D. Peterson, J. Liu, G. Fang, and D. L. Carroll, *Sol. Energy* **85**, 450 (2011).
- <sup>19</sup>R. Hausermann, E. Knapp, M. Moos, N. A. Reinke, T. Flatz, and B. Ruhstaller, *J. Appl. Phys.* **106**, 104507 (2009).
- <sup>20</sup>D. W. Sievers, V. Shrotriya, and Y. Yang, *J. Appl. Phys.* **100**, 114509 (2006).
- <sup>21</sup>Y. M. Nam, J. Huh, and W. H. Jo, *Sol. Energy Mater. Sol. Cells* **94**, 1118 (2010).
- <sup>22</sup>R. H. Bube and A. L. Fahrenbruch, *Advances in Electronics and Electron Physics* (Academic, New York, 1981), p. 163.
- <sup>23</sup>A. Cheknane, H. S. Hilal, F. Djeflal, B. Benyoucef, and J. P. Charles, *Microelectron J* **39**, 1173 (2008).
- <sup>24</sup>A. Shah, P. Torres, R. Tscharnner, N. Wyrsh, and H. Keppner, *Science* **285**, 692 (1999).
- <sup>25</sup>A. L. Fahrenbruch and J. Aranovich, *Solar Energy Conversion* (Springer-Verlag, New York, 1979), p. 257.
- <sup>26</sup>B. P. Rand, D. P. Burk, and S. R. Forrest, *Phys. Rev. B* **75**, 115327 (2007).
- <sup>27</sup>K. Vandewal, K. Tvingstedt, A. Gadisa, O. Inganas, and J. V. Manca, *Nat. Mater.* **8**, 904 (2009).
- <sup>28</sup>G. Li, V. Shrotriya, J. Huang, Y. Yao, T. Moriarty, K. Emery, and Y. Yang, *Nat. Mater.* **4**, 864 (2005).
- <sup>29</sup>Y. Li and Y. Zou, *Adv. Mater.* **20**, 2952 (2008).
- <sup>30</sup>A. Pivrikas, G. Juscaronka, A. J. Mozer, M. Scharber, K. Arlauskas, N. S. Sariciftci, H. Stubb, and R. Österbacka, *Phys. Rev. Lett.* **94**, 176806 (2005).
- <sup>31</sup>L. A. A. Pettersson, L. S. Roman, and O. Inganas, *J. Appl. Phys.* **86**, 487 (1999).
- <sup>32</sup>F. Monestier, J.-J. Simon, P. Torchio, L. Escoubas, F. Flory, S. Bailly, R. de Bettignies, S. Guillerez, and C. Defranoux, *Sol. Energy Mater. Sol. Cells* **91**, 405 (2007).
- <sup>33</sup>B. G. Wei, *Technical Physics Teaching* **16**, 17 (2008).
- <sup>34</sup>See Supplemental Material at <http://link.aps.org/supplemental/10.1103/PhysRevB.84.085206> for superimposed voltage; See Supplemental Material at <http://link.aps.org/supplemental/10.1103/PhysRevB.84.085206> for voltage when heterogeneous illumination; See Supplemental Material at <http://link.aps.org/supplemental/10.1103/PhysRevB.84.085206> for upper bound of voltage.
- <sup>35</sup>K. I. Ishibashi, Y. Kimura, and M. Niwano, *J. Appl. Phys.* **103**, 094507 (2008).
- <sup>36</sup>J. W. Liu, M. A. G. Namboothiry, and D. L. Carroll, *Appl. Phys. Lett.* **90**, 133515 (2007).
- <sup>37</sup>M. J. Currie, J. K. Mapel, T. D. Heidel, S. Goffri, and M. A. Baldo, *Science* **321**, 226 (2008).
- <sup>38</sup>C. Dominguez, I. Anton, and G. Sala, *Opt. Express* **16**, 14894 (2008).
- <sup>39</sup>K. Omer, H. Baruch, A. K. Eugene, and M. G. Jeffrey, *Appl. Phys. Lett.* **91**, 064101 (2007).
- <sup>40</sup>Y. Li, “*Open Photovoltaics Analysis Platform (OPVAP)*,” [<http://www.OPVAP.inwake.com>] (2011).